PHYSICAL REVIEW D **78,** 055019 (2008)

Exploring compressed supersymmetry with same-sign top quarks at the CERN Large Hadron Collider

Stephen P. Martin

Department of Physics, Northern Illinois University, DeKalb Illinois 60115, USA,
Fermi National Accelerator Laboratory, P.O. Box 500, Batavia Illinois 60510, USA,
and Kavli Institute for Theoretical Physics, University of California, Santa Barbara California 93106-4030, USA

(Received 6 August 2008; published 26 September 2008)

In compressed supersymmetry, a light top squark naturally mediates efficient neutralino pair annihilation to govern the thermal relic abundance of dark matter. I study the CERN LHC signal of same-sign leptonic top-quark decays from gluino and squark production, which follows from gluino decays to top plus stop followed by the stop decaying to a charm quark and the LSP in these models. Measurements of the numbers of jets with heavy-flavor tags in the same-sign lepton events can be used to confirm the origin of the signal. Summed transverse momentum observables provide an estimate of an effective superpartner mass, which is correlated with the gluino mass. Measurements of invariant mass endpoints from the visible products of gluino decays do not allow direct determination of superpartner masses, but can place constraints on them, including lower bounds on the gluino mass as a function of the top-squark mass.

DOI: 10.1103/PhysRevD.78.055019 PACS numbers: 14.80.Ly, 12.60.Jv, 14.65.Ha, 95.35.+d

I. INTRODUCTION

If supersymmetry [1] is the solution to the hierarchy problem associated with the small ratio of the electroweak scale to the Planck scale, then some of the superpartners should be discovered at the impending CERN Large Hadron Collider (LHC). While the essential idea of supersymmetry as a symmetry connecting fermion and boson degrees of freedom is quite predictive, the unknown features of the supersymmetry-breaking mechanism allow for a diverse variety of possibilities for the LHC signals of superpartner production and decay [2,3].

The purpose of this paper is to study some of the distinctive LHC signals particular to the "compressed supersymmetry" scenario proposed in Ref. [4], which is motivated both by the supersymmetric little hierarchy problem and by the cold dark-matter relic abundance obtained by WMAP, SDSS, and other experiments [5,6]. This model scenario follows from assuming that the ratio of the running gluino and W-ino mass parameters, M_3/M_2, is smaller than 1 near the grand unified theory (GUT) scale, unlike the assumption of the well-studied "minimal supergravity" (mSUGRA) framework. (Models with nonunified gaugino masses have recently attracted renewed interest (see, for example, [7–33]), due to their ability to incorporate novel LHC phenomenology and dark-matter physics.) As a result, the ratio of the physical masses of the heaviest and the lightest superpartners is much less than in mSUGRA, because the gluino mass feeds into the other superpartner masses by renormalization group evolution. Another characteristic feature is that the pair annihilation of the lightest supersymmetric particles (LSPs) in the early universe can naturally proceed dominantly through $\tilde{N}_1\tilde{N}_1 \to t\bar{t}$, mediated by top-squark exchange. This is due to the fact that the stop-LSP mass difference is naturally not too large, particularly in models that have enough top-squark mixing to evade the Higgs scalar boson mass bound from the CERN LEP.

In compressed supersymmetry, the superpartner masses are typically all less than 1 TeV in the available parameter space. This means that the initial evidence for supersymmetry should follow quickly from the classic jets with missing transverse energy ($E_T^{\rm miss}$) signal, as soon as the systematic difficulties associated with understanding missing energy as manifested in the LHC detectors are conquered. We can then turn our attention to those features of the signal that might distinguish it from the usual mSUGRA models. In much of the parameter space in compressed supersymmetry that predicts the observed thermal relic abundance of dark matter, the mass difference between the top squark and the neutralino LSP $\tilde{N}_1$ is less than 85 GeV, so that the flavor-preserving decays including $\tilde{t}_1 \to t\tilde{N}_1$ and $\tilde{t}_1 \to b\tilde{C}_1$ and $\tilde{t}_1 \to bW\tilde{N}_1$ are kinematically forbidden. In this paper, I will assume that the flavor-violating 2-body decay

$$\tilde{t}_1 \to c\tilde{N}_1 \tag{1.1}$$

dominates over the remaining possibility [34,35], the 4-body decay $\tilde{t}_1 \to bf\bar{f}'\tilde{N}_1$. (For more on this assumption, see the next section.) Assuming the top squark is lighter than the gluino, one has

$$\tilde{g} \to \begin{cases} t\tilde{t}_1^* & (50\%) \\ \bar{t}\tilde{t}_1 & (50\%), \end{cases} \tag{1.2}$$

due to the Majorana nature of the gluino, leading to

$$pp \to \tilde{g}\,\tilde{g} \to \begin{cases} tt\bar{c}\,\bar{c}\,\tilde{N}_1\tilde{N}_1 & (25\%) \\ \bar{t}\,\bar{t}\,cc\tilde{N}_1\tilde{N}_1 & (25\%) \\ t\bar{t}c\bar{c}\tilde{N}_1\tilde{N}_1 & (50\%). \end{cases} \tag{1.3}$$

When both of the same-sign top quarks of the first two cases decay leptonically, one obtains a distinctive detector signal of two same-sign leptons, two potentially b-tagged jets, two or more additional jets, and missing energy from the LSPs and neutrinos:

$$pp \to \ell^{\pm}\ell'^{\pm} bbjj + E_T^{\rm miss}. \tag{1.4}$$

This is a special case of the well-known same-sign dilepton signature for Majorana gluino (or gaugino) production in supersymmetry [36]. This LHC signal for gluino pairs was proposed and studied in some detail, in the context of models with much lighter top squarks ($m_{\tilde{t}_1} < m_t$), in Ref. [37]. Adding to this signal in compressed supersymmetry will be events in which squarks are produced, giving extra jets in the final state when they decay to the gluino. The presence of same-sign leptons provides for a strongly suppressed standard model background compared to other missing energy signals, and this is further aided by requiring two b-tagged jets.

In this paper, I will consider the properties of the LHC events that conform to this signal in compressed supersymmetry. (Other studies of the LHC phenomenology of compressed supersymmetry are found in [38,39].) Section II defines a model line for study, a one-parameter slice of model space with the free parameter corresponding to the gaugino mass scale. I also discuss some of the prominent properties of the superpartner mass spectrum of this model line that make it qualitatively different from mSUGRA models. Section III describes an event selection for the $\ell^{\pm}\ell'^{\pm} bbjj + E_T^{\rm miss}$, and the features of the resulting signal events. Section IV considers mass-estimating observables based on the scalar sum of transverse momentum of detector objects, while Sec. V studies kinematic endpoints of the invariant masses of visible products of the gluino decay. Section VI contains some concluding remarks.

II. A COMPRESSED SUPERSYMMETRY MODEL LINE

One simple realization of compressed supersymmetry is obtained by supposing that the running b-ino, W-ino, and gluino masses are parametrized at $M_{\rm GUT}$ by

$$M_1 = m_{1/2}(1 + C_{24}), \tag{2.1}$$

$$M_2 = m_{1/2}(1 + 3C_{24}), \tag{2.2}$$

$$M_3 = m_{1/2}(1 - 2C_{24}), \tag{2.3}$$

corresponding to an F-term source for supersymmetry breaking in a linear combination of the singlet and adjoint representations of $SU(5)$ [7–10]. Merely for simplicity, I also assume a common scalar mass m_0 and scalar trilinear coupling A_0, both at $M_{\rm GUT}$. The other parameters defining the model are $\tan\beta$ and the phase of the μ parameter, which is taken to be real. I use SOFTSUSY 2.0.11 [40] to generate the superpartner spectrum. To define the model line for study here, let

$$\begin{aligned} C_{24} &= 0.21, \qquad A_0/M_1 = -1, \\ \tan\beta &= 10, \qquad \mu > 0, \end{aligned} \tag{2.4}$$

with M_1 (or equivalently $m_{1/2}$) taken as the single varying parameter of the model line. (Here and in the following, M_1 is used to denote the running b-ino mass parameter at $M_{\rm GUT}$, not at the electroweak scale.) For each value of M_1, the parameter m_0 is obtained by imposing as a requirement that the predicted dark-matter relic abundance (obtained using the program MICROMEGAS 2.0.1 [41]) satisfies $\Omega_{\rm DM}h^2 = 0.11$ [5,6]. The resulting values of m_0 are not too large, ranging from 210 to 380 GeV (and always less than the W-ino and b-ino masses at the GUT scale) for the model line when the physical gluino mass is less than 1 TeV.

With strictly flavor-conserving boundary conditions for the soft supersymmetry-breaking interactions at the GUT scale, the 2-body decay $\tilde{t}_1 \to c\tilde{N}_1$ and the 4-body decay $\tilde{t}_1 \to bf\bar{f}'\tilde{N}_1$ would have roughly comparable partial decay widths on this model line. Using SDECAY [42], one finds that BR($\tilde{t}_1 \to bf\bar{f}'\tilde{N}_1$) would range from a few percent (for a small mass difference $m_{\tilde{t}_1} - m_{\tilde{N}_1} \approx 30$ GeV) to nearly 90% (for the largest mass difference of about 70 GeV).[1] However, the strict minimal flavor violation assumption on which this is based is notoriously unmotivated by theory, except in models with special features like gauge-mediated supersymmetry breaking. A small amount of nonminimal flavor violation results in the 2-body decay $\tilde{t}_1 \to c\tilde{N}_1$ dominating, as assumed here. Writing the effective stop-charm-neutralino interaction at the weak scale as $\mathcal{L} = -\tilde{t}_1^*(y_L c_L \tilde{N}_1 + y_R c_R \tilde{N}_1)$, I find that even for the worst-case point on the model line, BR($\tilde{t}_1 \to c\tilde{N}_1$) $>$ 95% provided that $(y_L^2 + y_R^2)^{1/2} > 8 \times 10^{-4}$. This would follow, for example, from a small off-diagonal right-handed up squark squared mass parameter at the GUT scale $m^2_{\tilde{c}_R^*\tilde{t}_R}/m_0^2 > 0.007$, with no danger of conflict with present flavor experiments.

The superpartner and Higgs boson mass spectrum for a representative point on the model line with $M_1 = 500$ GeV is shown in Fig. 1. The ratio of masses of the heaviest and lightest superpartners in this model is 3.6, almost a factor of 2 smaller than is obtainable in mSUGRA models even with small m_0. The neutralino LSP is heavier than the top quark, allowing $\tilde{N}_1\tilde{N}_1 \to t\bar{t}$. The top squark is the next-to-lightest superpartner. Another distinctive feature is that $\tilde{C}_1$

[1] The most important contribution to the 4-body decay partial width in this model line comes from the Feynman graph with virtual W and top-quark exchange, unlike in most other models considered in the literature (see, for example, [35,43,44]), where diagrams with W and chargino or slepton and chargino exchange dominate.

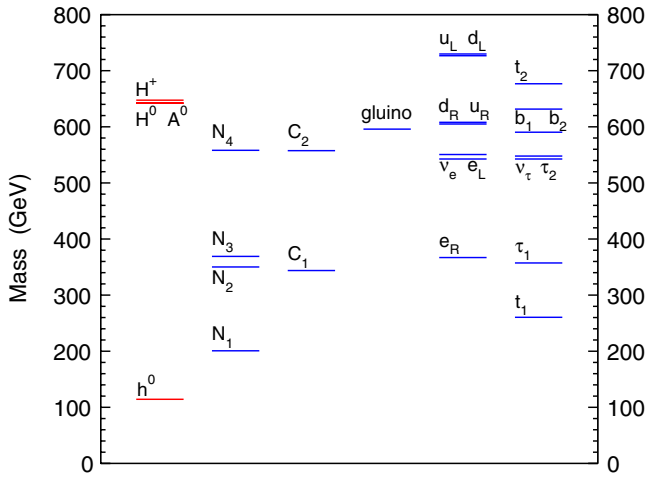

FIG. 1 (color online). The mass spectrum for a sample point on the model line described in the text, with $M_1 = 500$ GeV at the GUT scale, $C_{24} = 0.21$, $A_0/M_1 = -1$, $m_0 = 314$ GeV, $\mu = 361$ GeV, and $\tan\beta = 10$. The columns contain, from left to right, Higgs scalar bosons, neutralinos, charginos, the gluino, first and second family squarks and sleptons, and third family squarks and sleptons.

and $\tilde{N}_{2,3}$ are Higgsinolike states, due to the fact that μ is only 361 GeV, again much smaller than found in mSUGRA models for comparable gluino and squark masses. (The relatively small value of $|\mu|$ is a sign of the reduced fine-tuning found in models with a small ratio M_3/M_2 at the GUT scale as pointed out long ago in [11].) The heaviest neutralino and chargino states $\tilde{N}_4$ and $\tilde{C}_2$ are W-ino-like. The sleptons turn out to be too heavy to play a significant role in LHC physics.

The gluino always decays to a top and stop in this model, and the stop always decays to a charm quark and LSP. Other important decay modes are, for left-handed squarks,

$$\tilde{u}_L \to u\tilde{g}\ (71\%), \quad d\tilde{C}_2\ (13\%), \quad u\tilde{N}_4\ (6\%), \quad d\tilde{C}_1\ (6\%), \tag{2.5}$$

$$\tilde{d}_L \to d\tilde{g}\ (73\%), \quad u\tilde{C}_2\ (14\%), \quad d\tilde{N}_4\ (7\%), \quad u\tilde{C}_1\ (3\%), \tag{2.6}$$

and for right-handed squarks,

$$\tilde{u}_R \to u\tilde{N}_1\ (92\%), \quad u\tilde{g}\ (5\%), \quad u\tilde{N}_2\ (3\%), \tag{2.7}$$

$$\tilde{d}_R \to d\tilde{N}_1\ (85\%), \quad d\tilde{g}\ (12\%), \quad d\tilde{N}_2\ (3\%). \tag{2.8}$$

Thus left-handed squarks are a plenteous source of gluinos, while right-handed squarks mostly decay directly to the LSP. Subdominant decays produce some neutralinos and charginos, which nearly always decay into on-shell W, Z, and h bosons or through top squarks. For the Higgsinolike states

$$\tilde{N}_2 \to h\tilde{N}_1\ (90\%), \quad Z\tilde{N}_1\ (10\%), \tag{2.9}$$

$$\tilde{N}_3 \to h\tilde{N}_1\ (97\%), \quad Z\tilde{N}_1\ (3\%), \tag{2.10}$$

$$\tilde{C}_1 \to b\tilde{t}_1\ (91\%), \quad W\tilde{N}_1\ (9\%), \tag{2.11}$$

and for the heavier, W-ino-like states

$$\tilde{N}_4 \to W\tilde{C}_1\ (51\%), \quad h\tilde{N}_2\ (20\%), \quad Z\tilde{N}_3\ (20\%), \quad t\tilde{t}_1\ (8\%), \tag{2.12}$$

$$\tilde{C}_2 \to W\tilde{N}_2\ (30\%), \quad W\tilde{N}_3\ (21\%), \quad Z\tilde{C}_1\ (25\%), \quad h\tilde{C}_1\ (21\%). \tag{2.13}$$

An important consequence of these decays is that one cannot find dilepton mass edges of the type used in [45–49] to obtain information about the superpartner mass spectrum. The only isolated leptons come from on-shell W and Z decays, since 2-body spoiler decays are always allowed. Furthermore, sleptons completely decouple from the cascade decays, because they are too heavy. These features are qualitatively maintained along the entire model line.

Varying M_1, one finds that $M_1 > 417$ GeV at the GUT scale is required to satisfy the LEP bound on the Higgs mass, taken here to be $m_h > 113$ GeV because of the theoretical uncertainty on the Higgs mass prediction. As M_1 increases, the gluino and LSP masses increase approximately in direct proportion, while the top-squark mass stays between 30 and 70 GeV heavier than the neutralino LSP. This is shown in Fig. 2, which plots the mass difference $m_{\tilde{t}_1} - m_{\tilde{N}_1}$ as a function of $m_{\tilde{g}}$ for the model line.

The bulge region where the stop-LSP mass difference is relatively large, with $m_{\tilde{g}}$ between about 525 and 650 GeV, is characterized by having $\tilde{N}_1\tilde{N}_1 \to t\bar{t}$ due to $\tilde{t}_1$ exchange as the dominant annihilation effect in determining the dark-matter thermal relic abundance. Note that varying m_0 to obtain $\Omega_{\rm DM}h^2$ anywhere within the allowed range 0.11 ± 0.02 would not change the fact that $m_{\tilde{t}_1} - m_{\tilde{N}_1} < m_W + m_b$ for this model line. This stop-mediated annihilation region is continuously connected in parameter space to more fine-tuned models in which the $\tilde{t}_1$, $\tilde{N}_1$ mass difference is just right to allow efficient stop-neutralino coannihilations,[2] for $m_{\tilde{g}}$ less than about 525 GeV and greater than about 650 GeV. An important consequence of the larger stop-LSP mass difference in the dark-matter annihilation-to-tops bulge region is that the LHC signal efficiency will be increased compared to the coannihilation regions on

[2]An even more fine-tuned stop-neutralino coannihilation region can also be found [50] in mSUGRA models.

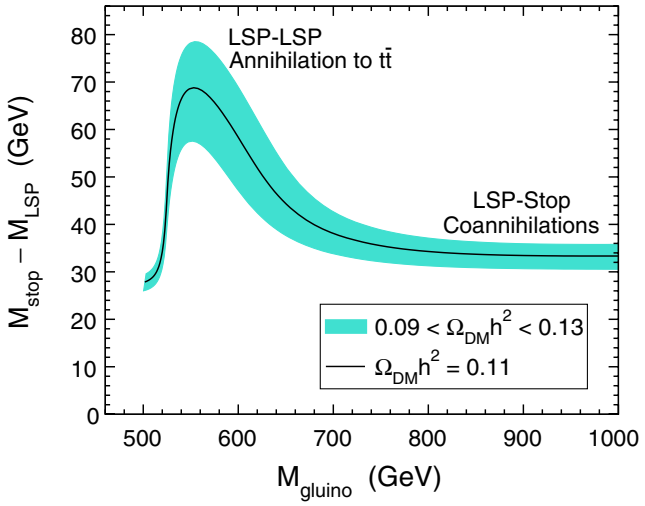

FIG. 2 (color online). The mass difference $m_{\tilde{t}_1} - m_{\tilde{N}_1}$ as a function of $m_{\tilde{g}}$, for the model line described in the text. The solid line is the model line with $\Omega_{\rm DM}h^2 = 0.11$, and the shaded region denotes the approximate region favored by the thermal relic abundance constraints. The model line is cut off on the left by the LEP2 Higgs mass constraint.

either side, since the jets from the decay $\tilde{t}_1 \to c\tilde{N}_1$ tend to have higher p_T.

The superpartner production cross sections are dominated by gluino and squark production. The next-to-leading order total cross sections for this model line are shown in Fig. 3, computed using PROSPINO2 [51].

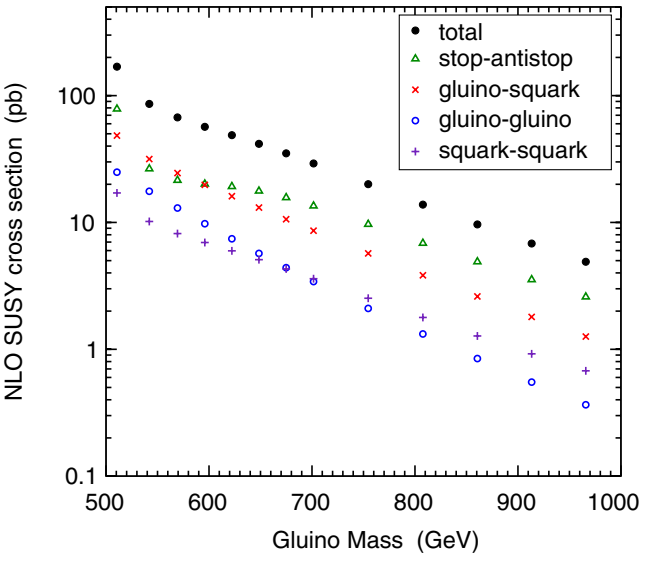

FIG. 3 (color online). The next-to-leading order production cross section for superpartner pairs in pp collisions at $\sqrt{s} = 14$ TeV for selected points along the model line described in the text, as a function of the gluino mass. PROSPINO2 [51] was used. The most important contributions, from stop pair production ($\tilde{t}_1\tilde{t}_1^*$), gluino-squark production ($\tilde{g}\,\tilde{q}$ and $\tilde{g}\tilde{q}^*$), gluino pair production ($\tilde{g}\,\tilde{g}$), and squark pair production ($\tilde{q}\,\tilde{q}$ and $\tilde{q}\tilde{q}^*$ and $\tilde{q}^*\tilde{q}^*$), are also shown separately.

The largest single source of supersymmetric events is $pp \to \tilde{t}_1\tilde{t}_1^*$, which is of order 25 pb throughout the bulge region, and falls rather slowly with the gluino mass along the model line. However, this leads to the very difficult signal of two often low-p_T charm jets and little missing energy. I have checked that after realistic cuts to remove QCD and detector backgrounds (see, for example, [3,52]), the low efficiency of the $\tilde{t}_1\tilde{t}_1^*$ signal will lead to it being buried beneath the other squark and gluino sources, so it is not possible to infer the existence of the light top squark from this direct production process. The total gluino-squark associated production $pp \to \tilde{g}\,\tilde{q}$ plus $\tilde{g}\tilde{q}^*$, summed over quark flavors, is of order tens of picobarns throughout the bulge region. Gluino pair production and (anti-)squark pair production both contribute of order 10 pb in the bulge region, with the former falling somewhat more steeply with increasing mass. The production and decays of gluinos and squarks in this scenario should easily allow for early discovery lepton + jets + $E_T^{\rm miss}$ channels (see, for example, Refs. [2,3,53] for comparable mSUGRA studies) at the LHC.

Sleptons decouple from practical LHC physics in many compressed supersymmetry models, and, in particular, for the model line studied here. For example, for the model line point with $M_1 = 500$ GeV shown in Fig. 1, the total direct production cross section of sleptons and sneutrinos before any cuts or efficiencies is only about 6 fb, compared to much larger backgrounds from WW production and other sources. As noted above, sleptons also extremely efficiently decouple from decay chains of heavier superpartners. Charginos and neutralinos (other than the LSP) do appear, but only in subdominant decay modes of the squarks. Their direct production rates are quite small compared to the gluino and squark rates. For example, for the model shown in Fig. 1, one obtains a total of (129, 41, 32) fb for, respectively, ($\tilde{C}_i^{\pm}\tilde{N}_j$, $\tilde{C}_i^{+}\tilde{C}_j^{-}$, $\tilde{N}_i\tilde{N}_j$) production. Neutralinos and charginos produced in association with gluinos and squarks add another 500 fb. These rates are quite small compared to the 56 pb total gluino and squark production rate, and involve a wide variety of dissimilar final states without strong distinguishing features. Furthermore, these do not yield dilepton mass edges, as noted above. Unfortunately, finding out any information about the superpartners other than the squarks, gluino, and LSP from direct observation appears to be a daunting challenge at the LHC in this scenario.

There are several ways of gaining information about the gluino and squark mass spectrum from the early discovery inclusive jets + leptons + $E_T^{\rm miss}$ signal, including, for example, m_{T2} and similar variables [54,55] and the multiplicity of b-tagged jets. However, the presence of non-negligible backgrounds that will have to be understood from LHC data puts these methods beyond the scope of the present paper. Instead, I will concentrate on tools that

use the lower rate but potentially very low-background signal with same-sign dileptons.

III. SIGNAL FROM SAME-SIGN LEPTONIC TOP DECAYS

To define a signal for same-sign $\ell^{\pm}\ell'^{\pm}bbjj + E_T^{\rm miss}$ events, I used MADGRAPH/MADEVENT [56] for event generation, and interfaced to PYTHIA [57] and then PGS4 [58] for detector simulation using CMS-like parameters. Events are selected by requiring the following from objects generated by PGS:

(i) exactly two same-sign isolated leptons ($\ell = e,\ \mu$) with $p_T > 20$ GeV and $|\eta| < 2.4$.
(ii) at least two b-tagged jets each with $p_T > 50$ GeV (with $|\eta| < 1.75$ required by PGS).
(iii) at least two more jets with $p_T > 50$, 35 GeV (with $|\eta| < 3.1$ required by PGS).
(iv) at least one pairing of each of the two leptons with a distinct b-tagged jet, with each pair having invariant mass consistent with leptonic top decay: $m(b\ell) < 160$ GeV.
(v) $E_T^{\rm miss} > 100$ GeV.

(These cuts are very similar to those used in Ref. [37].) The uncorrected jet momenta from PGS are used. The reason for the cut on the $b\ell$ invariant mass is that the parton-level kinematic endpoint is

$$m(b\ell)_{\rm max} = \sqrt{m_t^2 - m_W^2}, \tag{3.1}$$

nominally about 153 GeV using $m_t = 172.7$ GeV. I use the higher value of 160 GeV for the cut in order to partially take into account the effects of smearing of the b-jet energies. The b tag is actually a heavy-flavor tag, which in PGS has an efficiency for high-p_T central jets of approximately 50% for true b jets, 13% for c jets, and 1% for g, u, d, s jets. Each of the leptons and jets are required to be isolated from each other by $\Delta R = \sqrt{(\Delta\phi)^2 + (\Delta\eta)^2} > 0.4$. Also, muons that are not isolated from a jet are absorbed into the jet, if the summed p_T (excluding the muon itself) in a cone of $\Delta R = 0.4$ around the muon exceeds 5 GeV, or if the ratio of the p_T in a 3×3 grid of calorimeter cells around the muon to the p_T of the muon itself exceeds 0.1.

The cross section after these cuts for LHC collisions with $\sqrt{s} = 14$ TeV is shown in Fig. 4, for points along the model line. Also shown are the two largest contributions, from $\tilde{g}\,\tilde{g}$ production and $\tilde{g}\,\tilde{q}$ production.

The efficiency for the $\tilde{g}\,\tilde{g}$ part of the signal is about 0.04%. Most of the $\tilde{g}\,\tilde{q}$ contribution to the signal is due to production of a left-handed squark in association with a gluino, since right-handed squarks usually decay directly to the LSP and the corresponding quark. The cross section after cuts is between 5 and 15 fb for gluino masses less than

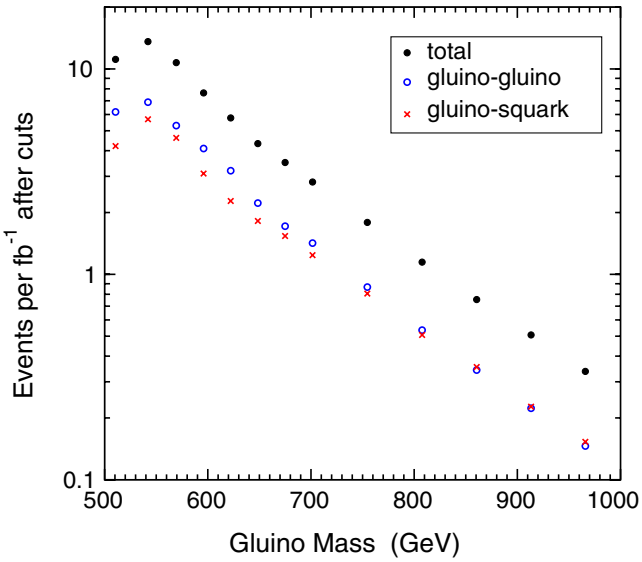

FIG. 4 (color online). The number of LHC signal events with two same-sign leptons, two b tags, and two additional jets, per fb^{-1}, after the cuts described in the text, for the model line described in Sec. II.

640 GeV, corresponding to the bulge region where stop-mediated annihilation to top quarks dominates the dark-matter annihilation in the early universe. For comparison, Ref. [37] found backgrounds totaling less than 0.5 fb, using very similar cuts (although a different event generation and detector simulation). Therefore, strong evidence for this source of supersymmetric events might be obtained with as little as a few fb^{-1}, depending on the gluino mass and, to a lesser extent, the squark masses. This of course presumes that the backgrounds can be well understood, and that wrong-sign assignments of lepton charges in e.g. $t\bar{t}$ production are indeed not large and irreducible. In the following, I will optimistically assume this to be the case, and neglect backgrounds.

Note that the cross section after cuts is actually lower for the lowest-mass point in Fig. 4 with $M_1 = 425$ GeV and $m_{\tilde{g}} = 511$ GeV than for the next-higher mass point with $M_1 = 450$ GeV and $m_{\tilde{g}} = 542$ GeV. This occurs for two main reasons. First, the efficiency is lower for $M_1 = 425$ GeV because of the much smaller stop-LSP mass difference, as noted in Fig. 2. Second, the $M_1 = 450$ point has much larger branching fractions for right-handed squarks to decay into gluinos, adding to the signal.

[The contribution of right-handed squarks declines again for heavier masses, and is eliminated by kinematics for points on the model line with $m_{\tilde{g}}$ larger than about 600 GeV. The branching ratios for $\tilde{d}_R \to d\tilde{g}$ and $\tilde{u}_R \to u\tilde{g}$ are (46%, 38%, 12%) and (21%, 16%, 5%), respectively, for the model line points with $M_1 = (450, 475, 500)$ GeV. For all other model line points shown in Figs. 3 and 4, the branching ratios of $\tilde{q}_R \to q\tilde{g}$ are negligible.]

To give an idea of the characteristics of the signal events, Fig. 5 shows the $E_T^{\rm miss}$, lepton p_T, and jet p_T (with and without b tags) distributions for the events that pass the cuts, given 100 fb^{-1} of data for a representative model with $M_1 = 475$ GeV ($m_{\tilde{g}} = 569$ GeV).

Clearly, raising the $E_T^{\rm miss}$ cut much farther above 100 GeV would have a significant unfortunate effect on the signal, even for heavier masses. The same is true for the subleading lepton and jet p_T's. On the other hand, there is considerably more room to raise the cuts on the leading lepton and jet p_T's without a huge effect on the signal, should that prove necessary to reduce backgrounds. Because of the practical difficulties that are anticipated in commissioning $E_T^{\rm miss}$ at the LHC, it is also tempting to consider dropping that cut altogether, since the same-sign dileptons and jet cuts alone might be enough to distinguish the signal from background. This may be, but Fig. 5 shows that the benefit accrued to the signal cross section from relaxing the $E_T^{\rm miss}$ cut below 100 GeV is limited, especially for the critical case of models with heavier gluinos, so for the purposes of the present analysis it will be kept.

The frequency of heavy-flavor-tagged jets in the signal sample can help to confirm that the signal is really due to gluino pairs decaying to stops that in turn decay to charm quarks and LSPs. The number of events with 2, 3, 4, or 5 heavy-flavor-tagged jets is shown in Fig. 6 for the point on the model line with $M_1 = 500$ GeV, for 100 fb^{-1}. Also included is the breakdown of these events into tight b tags as reported by PGS, with efficiencies for central high-p_T jets of approximately 40% for true b jets, 9% for c jets, and 0.1% for g, u, d, s jets.

As a simpleminded check, one can assume that the $m(b\ell) < 160$ GeV requirement preselects only events that have the true b jets tagged, so that additional heavy-flavor tags come from the true charm jets, and the numbers of events with 2, 3, 4, and 5 heavy-flavor tags should be roughly in the proportion $n_2{:}n_3{:}n_4{:}n_5 = (1 - P_c)^2{:}2P_c(1 - P_c){:}P_c^2{:}0$, where P_c is the probability of a true charm jet getting a heavy-flavor tag. Using $n_2 = 930$ for the example in Fig. 6, and $P_c = 0.13$, one would predict $n_3 = 278$ and $n_4 = 21$ and $n_5 = 0$, in not unreasonable agreement for such a naive estimate with the actual finding of $n_3 = 299$ and $n_4 = 37$ and $n_5 = 1$. This information can be used to clearly distinguish the scenario under study here from similar ones in which the stop-LSP mass difference is large enough to allow $\tilde{t}_1 \to bW\tilde{N}_1$, or

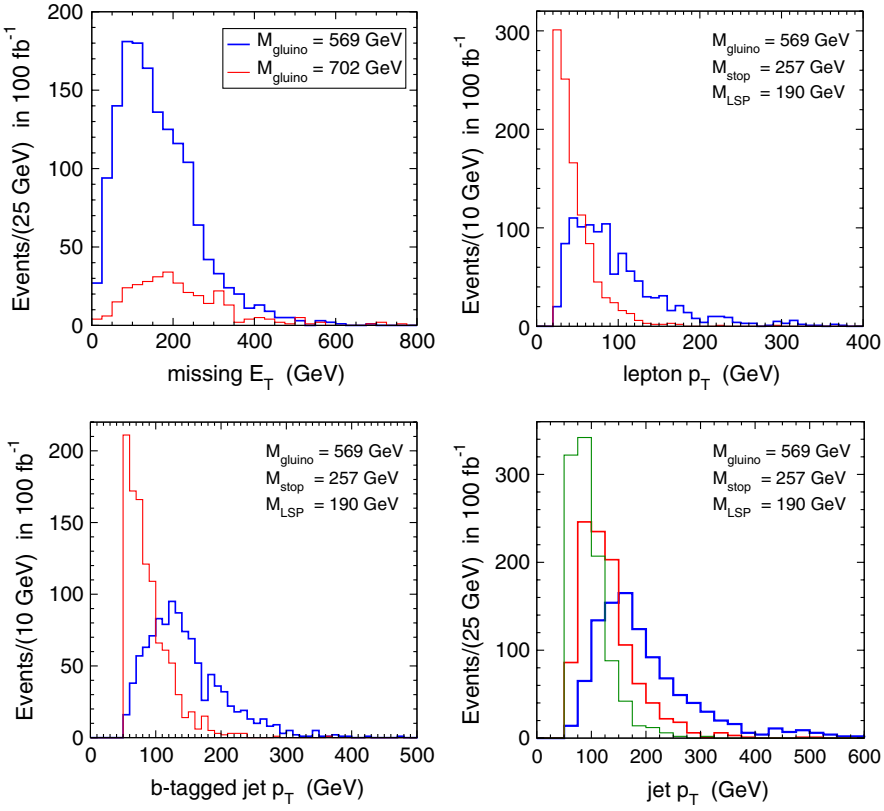

FIG. 5 (color online). Representative transverse momentum distributions for $\ell^{\pm}\ell'^{\pm}bbjj + E_T^{\rm miss}$ events from 100 fb^{-1} of superpartner production, after the cuts described in the text. The upper left panel shows the $E_T^{\rm miss}$ distribution (here without the $E_T^{\rm miss}$ cut) for two points on the model line with $m_{\tilde{g}} = 569$ and 702 GeV. The upper right panel shows the leading and subleading lepton p_T distributions for the model with $m_{\tilde{g}} = 569$, and the lower panels show the leading and subleading b-jet distributions (left) and the three leading jet distributions (right) for the same model point.

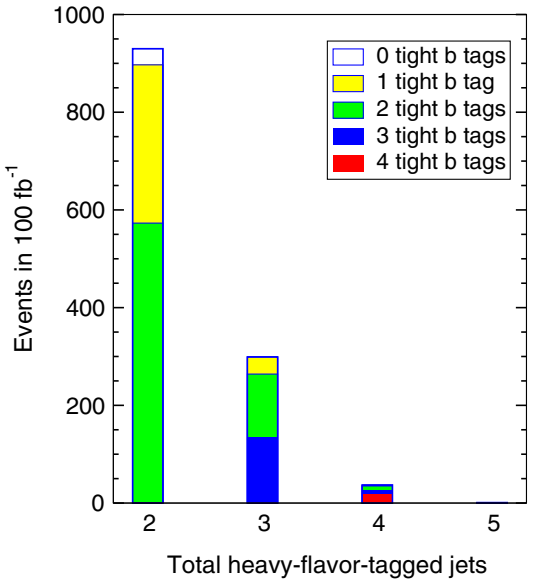

FIG. 6 (color online). The number of signal events after cuts in 100 fb^{-1} with exactly 2, 3, 4, or 5 PGS heavy-flavor-tagged jets, for the point on the model line described in Sec. II with $M_1 = 500$ GeV, resulting in $m_{\tilde{g}} = 596$ GeV. The breakdown into numbers of tight b tags is also shown. The relative frequencies of heavy-flavor tags provide additional evidence for the $\tilde{g} \to t\tilde{t}_1$ and $\tilde{t}_1 \to c\tilde{N}_1$ interpretation of the signal.

where strict minimal flavor violation leads to a dominant or competitive 4-body decay $\tilde{t}_1 \to bf\bar{f}'\tilde{N}_1$, either of which would lead instead to a parton-level same-sign dilepton signature of

$$pp \to \ell^{\pm}\ell'^{\pm} bbbbjjjj + E_T^{\rm miss}. \tag{3.2}$$

In this case, one would clearly expect many more events with 3, 4, and even 5 or more (since half of the hadronic W decays will result in a true charm jet) heavy-flavor tags relative to the number with 2 tags, compared to the situation in Fig. 6. Measuring the numbers of heavy-flavor tags within the $\ell^{\pm}\ell'^{\pm} bbjj + E_T^{\rm miss}$ signal sample can therefore establish whether $m_{\tilde{t}_1} - m_{\tilde{N}_1} < 85$ GeV. Of course, the specific numbers for heavy-flavor tagging in the actual LHC detector environments might be quite different from those assumed here, but the principle should still apply.

In the remainder of this paper, I will examine some strategies for obtaining information about the gluino, squark, and LSP mass spectrum. Note that variables like m_{T2} [54,55] are hampered, for the same-sign dilepton event topology, by the inevitable presence of two neutrinos with unknown momenta in addition to the two LSPs in each event. I have therefore not attempted the difficult task of seeing whether this can give useful information when applied to the same-sign lepton sample. The definite absence of dilepton mass edges eliminates another commonly used tool [45–49] for reconstructing superpartner decay chains. Instead, I will consider mass estimators that use scalar-summed transverse momenta and single-lepton mass edges from visible gluino decay products.

IV. MASS ESTIMATORS FROM SCALAR-SUMMED TRANSVERSE MOMENTA

One of the most important efforts in a future LHC analysis of supersymmetry will be to obtain measurements, or at least estimates, of the superpartner masses. The purpose of this section is to consider observables that can serve as estimators of the masses of the superpartners produced, using scalar sums of the lepton and jet p_T's. There has been considerable effort in this area, often using the observables H_T and $M_{\rm eff}$ for events with jets and $E_T^{\rm miss}$. Here, I will study the prospects for using similar observables, but in the hopefully cleaner context of the $\ell^{\pm}\ell'^{\pm} bbjj + E_T^{\rm miss}$ signal discussed in the previous section. To this end, consider four mass estimators defined by

$$M_A = \sum_n p_T(j_n) + \sum_{n=1,2} p_T(\ell_n) + E_T^{\rm miss}, \tag{4.1}$$

$$M_B = \sum_{n=1,2,3,4} p_T(j_n) + \sum_{n=1,2} p_T(\ell_n) + E_T^{\rm miss}, \tag{4.2}$$

$$M_C = \sum_n p_T(j_n) + \sum_{n=1,2} p_T(\ell_n), \tag{4.3}$$

$$M_D = \sum_{n=1,2,3,4} p_T(j_n) + \sum_{n=1,2} p_T(\ell_n), \tag{4.4}$$

where the jet labels are ordered by $p_T(j_1) > p_T(j_2) > p_T(j_3) > \ldots$. As usual, the idea is that the transverse momenta of the decay products should be approximately linear in the mass of the pair of heavy particles produced. The first observable, M_A, simply sums over all visible object p_T's and the $E_T^{\rm miss}$. The second observable, M_B, is motivated by the ideas that the sum over only the leading four jets should be less sensitive to theoretical uncertainties due to extra jets from the underlying event, and that the signal includes at least four quark partons. The other two observables, $M_{C,D}$, are the same as $M_{A,B}$ except that $E_T^{\rm miss}$ is not included. This is motivated by the fact that $E_T^{\rm miss}$ may be particularly difficult to obtain accurately, especially in early running of the LHC.

Using the same event selection criterion as in the previous section, the distributions for these four mass estimators are shown in Fig. 7, for 100 fb^{-1} of data with three representative points on the model line defined in Sec. II with $m_{\tilde{g}} = 542$, 596, and 675 GeV.

Even from these coarse-binned distributions, it is apparent that the shapes of the distributions are distinguishable from each other.

To determine a sharper empirical relation between these mass estimators and the superpartner mass scale, I per-

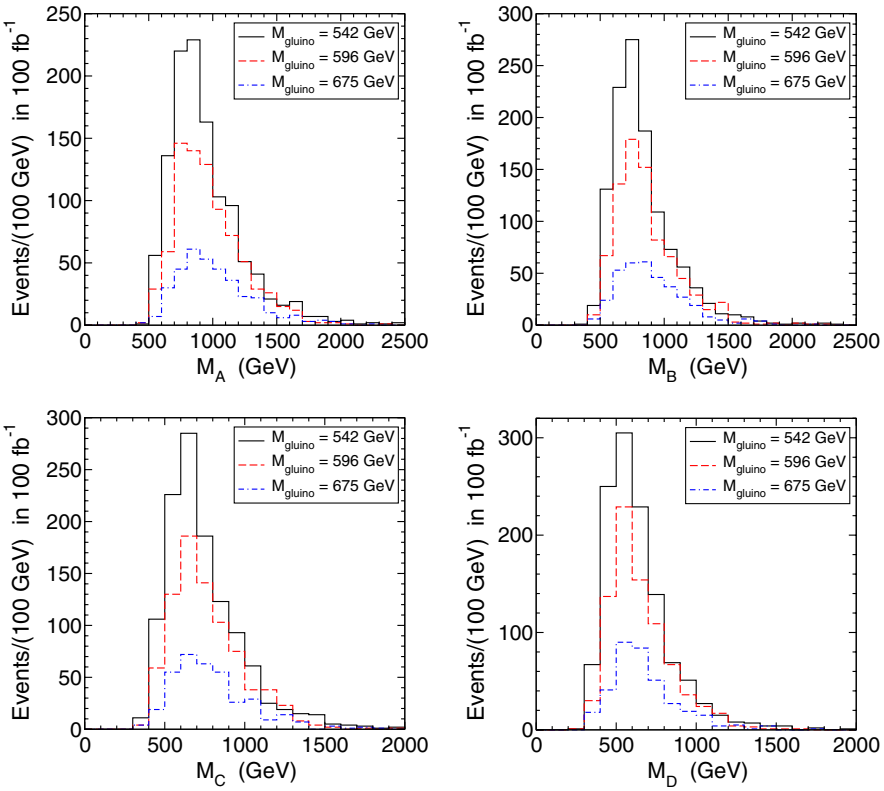

FIG. 7 (color online). Distributions for the mass estimators $M_{A,B,C,D}$ defined by Eqs. (4.1), (4.2), (4.3), and (4.4), for 100 fb^{-1} of events for three models along the model line described in Sec. II, with $M_1 = 450$, 500, and 575 GeV.

formed an unbinned maximum likelihood fit to 100 fb^{-1} of generated events for each of nine model points. Because the distributions of M_X (for $X = A, B, C, D$) are clearly far from Gaussian, better results are obtained by fitting them instead to the class of functions known as generalized inverse Gaussian distributions (with $x = M_X$):

$$f(x) = \frac{1}{n}(x - x_0)^{-c} \exp\left[-\frac{b(x - x_0 - a)^2}{2(x - x_0)}\right]. \quad (4.5)$$

Here a, b, and c are the fit parameters, and x_0 is the minimum of the distribution following simply from the jet and lepton p_T and $E_T^{\rm miss}$ cuts. (In the present analysis, x_0 is equal to 325 GeV for $X = A, B$ and 225 GeV for $X = C, D$.) The normalization condition

$$\int_{x_0}^{\infty} f(x)dx = 1 \quad (4.6)$$

implies that

$$\ln(n) = ab + (1 - c)\ln(a) + \ln[2K_{c-1}(ab)], \quad (4.7)$$

with $K_i(z)$ the modified Bessel function of the second kind. The peak of each distribution, defined as the value where $df/dx = 0$, is then obtained as

$$M_X^{\rm peak} = x_0 + (\sqrt{a^2b^2 + c^2} - c)/b, \quad (4.8)$$

where a, b, c are set equal to their best-fit values[3] after maximizing the log likelihood function.

Performing a linear regression (with the variance for each model taken inversely proportional to the number of events found in 100 fb^{-1}) gives relationships between the mass estimators $M_X^{\rm peak}$ and the gluino mass:

$$M_{\tilde g} = 1.693 M_A^{\rm peak} - 776 \text{ GeV}, \quad (4.9)$$

$$= 1.733 M_B^{\rm peak} - 634 \text{ GeV}, \quad (4.10)$$

$$= 2.274 M_C^{\rm peak} - 825 \text{ GeV}, \quad (4.11)$$

$$= 2.422 M_D^{\rm peak} - 676 \text{ GeV}. \quad (4.12)$$

The comparison between the linear fits and the values obtained for the individual models are shown in Fig. 8.

The smaller slopes of the $M_{\tilde g}$ vs $M_{A,B}^{\rm peak}$ lines would seem to make them more useful as mass estimators than $M_{C,D}^{\rm peak}$,

[3]The best fits obtained in the following almost always turn out to have c very close to 3/2, corresponding to the special case known as an ordinary inverse Gaussian distribution (not to be confused with a normal Gaussian distribution). I do not know the explanation for this.

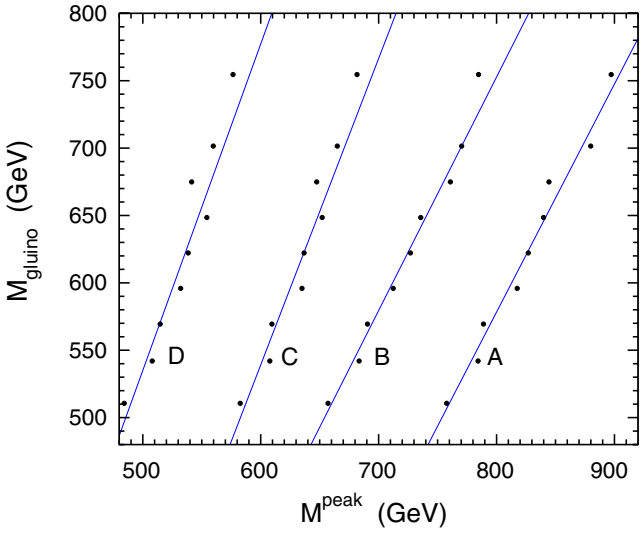

FIG. 8 (color online). The gluino mass is compared to the fitted peak values of the distributions of the mass estimators $M_{A,B,C,D}$ defined by Eqs. (4.1), (4.2), (4.3), and (4.4). Results for 100 fb^{-1} of events for each of nine individual models along the model line are shown as black dots, together with the best-fit lines, Eqs. (4.9), (4.10), (4.11), and (4.12).

although this depends crucially on the presently unknown quality of the $E_T^{\rm miss}$ determination.

In general, the mass estimators might be expected to be roughly proportional to $M_{\rm eff} = M_{\rm SUSY} - m^2_{\tilde N_1}/M_{\rm SUSY}$, where $M_{\rm SUSY}$ is a signal cross-section weighted average of the superpartner masses, in this case the gluino and left-handed squark masses. In models with a slightly larger $m_{\tilde q_R} - m_{\tilde g}$ mass difference, the decay $\tilde q_R \to q\tilde g$ would be more important, and $m_{\tilde q_R}$ would be weighted more strongly into $M_{\rm SUSY}$. In the model line under study, the LSP mass and the gluino mass are very nearly proportional, and the squark masses are also tightly correlated with the gluino mass. In general, since the presence of the signal depends crucially on the Majorana nature of the gluino, this method should be useful to obtain a rough estimate of the gluino mass, albeit with some mild model assumptions.

V. ENDPOINTS OF VISIBLE GLUINO DECAY PRODUCTS

Another method that can be used to gain information about the superpartner masses is to look at the invariant mass distributions of identified visible products of the gluino decay. This method has already been extensively studied in Ref. [37], in a situation similar to the present one, but with a relatively much lighter top squark and LSP, and taking the squarks to be much heavier. In the model scenario under study here, the presence of a large component of $\tilde g\,\tilde q \to \tilde g\,\tilde g\,q$ in the signal causes a significant additional source for confusion in identifying the jets following from the gluino decay.

The parton-level kinematic endpoints from the decay $\tilde g \to t\tilde t_1$ followed by $\tilde t_1 \to c\tilde N_1$ and $t \to b\ell\nu$ are [37]

$$m^2(\ell c)_{\rm max} = \tfrac{1}{2}(1 - m^2_{\tilde N_1}/m^2_{\tilde t_1})[m^2_{\tilde g} - m^2_{\tilde t_1} - m^2_t + \lambda^{1/2}(m^2_{\tilde g}, m^2_{\tilde t_1}, m^2_t)], \quad (5.1)$$

$$m^2(bc)_{\rm max} = (1 - m^2_W/m^2_t)m^2(\ell c)_{\rm max}, \quad (5.2)$$

$$m^2(b\ell c)_{\rm max} = m^2(\ell c)_{\rm max} + m^2_t - m^2_W, \quad (5.3)$$

where $\lambda(x, y, z) = x^2 + y^2 + z^2 - 2xy - 2xz - 2yz$. Note that these endpoints are not independent; knowing any one of them yields the others, given the known masses of the top quark and W boson. (The widths of the particles, and the mass of the bottom quark, are neglected here.) The corresponding distributions [37] for the model depicted in Fig. 1 with $m_{\tilde g} = 596$ GeV, $m_{\tilde t_1} = 260.5$ GeV, and $m_{\tilde N_1} = 200.8$ GeV are shown in Fig. 9.

Reference [37] performed fits to the shapes of bc and ℓc mass distributions, finding that the quality of the fits was made worse by leptons from taus in the top decays, among other effects. In the present case, there is a serious additional (and, in practice, unknown) effect on the shape from wrong jet assignments due to the presence in some events of $\tilde q_L \to q\tilde g$, and to a lesser extent $\tilde q_R \to q\tilde g$. Therefore, it is probably more robust to concentrate on the endpoints of the distributions. From Fig. 9 one sees that the $m(\ell c)$ distribution is extremely shallow near the endpoint, mak-

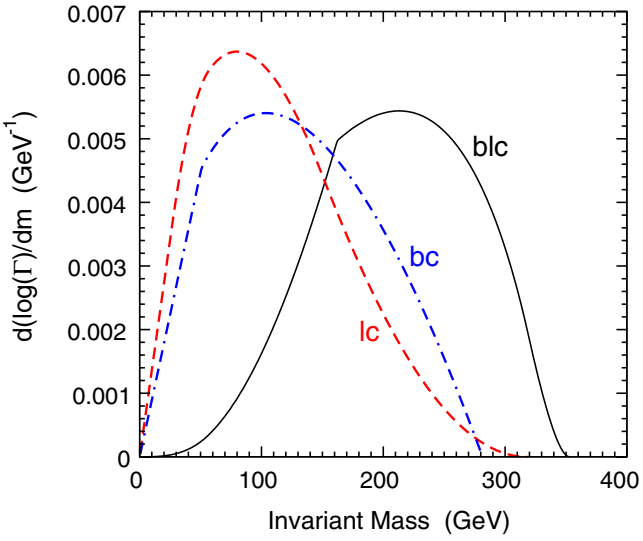

FIG. 9 (color online). The parton-level predictions for the distributions of the invariant masses $m(b\ell c)$, $m(bc)$, and $m(\ell c)$, for the decay $\tilde g \to t\tilde t_1$ followed by $\tilde t_1 \to c\tilde N_1$ and $t \to bW$ and $W \to \ell\nu$. The masses used are $m_{\tilde g} = 596$ GeV, $m_{\tilde t_1} = 261$ GeV, and $m_{\tilde N_1} = 201$ GeV, corresponding to a point on the model line with $M_1 = 500$ GeV. The endpoints of the distributions are at $m(b\ell c) = 354$ GeV and $m(bc) = 283$ GeV and $m(\ell c) = 320$ GeV.

ing it very difficult to determine the endpoint from data. The $m(bc)$ and $m(b\ell c)$ distributions are much steeper near their respective endpoints, so I will only consider them. It should be noted that different events contribute to the near-endpoint regions of these two distributions, even though the positions of the endpoints are algebraically related.

To mitigate the problem of wrong jet assignments, I use a subset of events selected by the procedure described in Sec. III, with the additional constraint that the pairing of the two leptons with b-tagged jets consistent with top decays [$m(b\ell) < 160$ GeV] is *unique*. (This reduces the signal efficiency by about a factor of 3.) For each $b\ell$ pair, the putative charm jet is taken to be the one with the smallest value of $m(b\ell c)$ selected from among those with $p_T > 35$ GeV. This selection means that far below the endpoints, there may well be many wrong assignments (both from extra jets in the underlying event and from jets produced in squark decays being assigned to the charm jet role), but near the endpoints the assignments are made correctly with greater frequency.

Results for the $m(b\ell c)$ and $m(bc)$ distributions selected in this way are shown in Figs. 10 and 11 for several

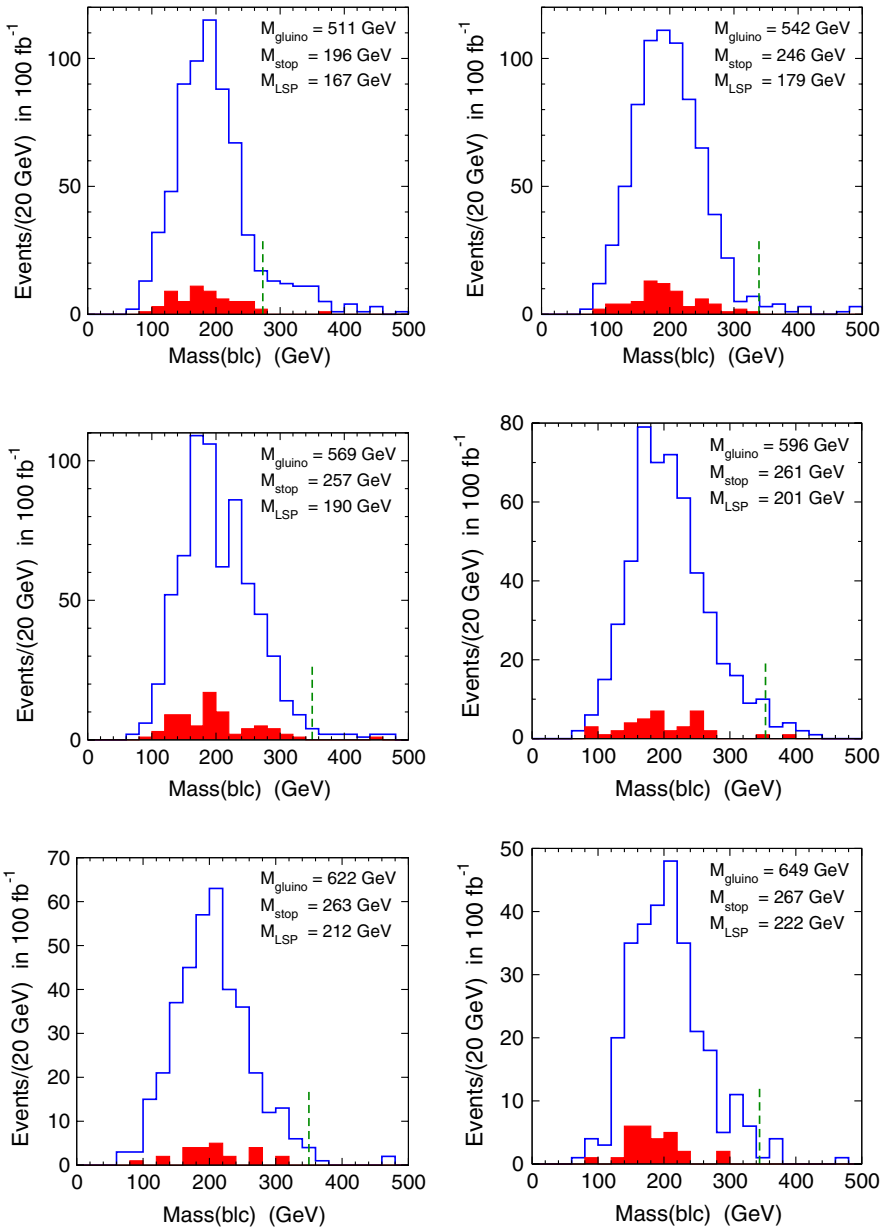

FIG. 10 (color online). The distributions of $m(b\ell c)$ for six points on the model line described in Sec. II with $M_1 = 425$, 450, 475, 500, 525, and 550 GeV. The nominal endpoints, indicated by the dashed vertical lines, are given by Eq. (5.2) as, respectively, $m(b\ell c)_{\rm max} = 273$, 339, 350, 354, 350, and 345 GeV. The solid histograms show the portion of the signal for which the putative c jet has a heavy-flavor tag or a soft muon tag.

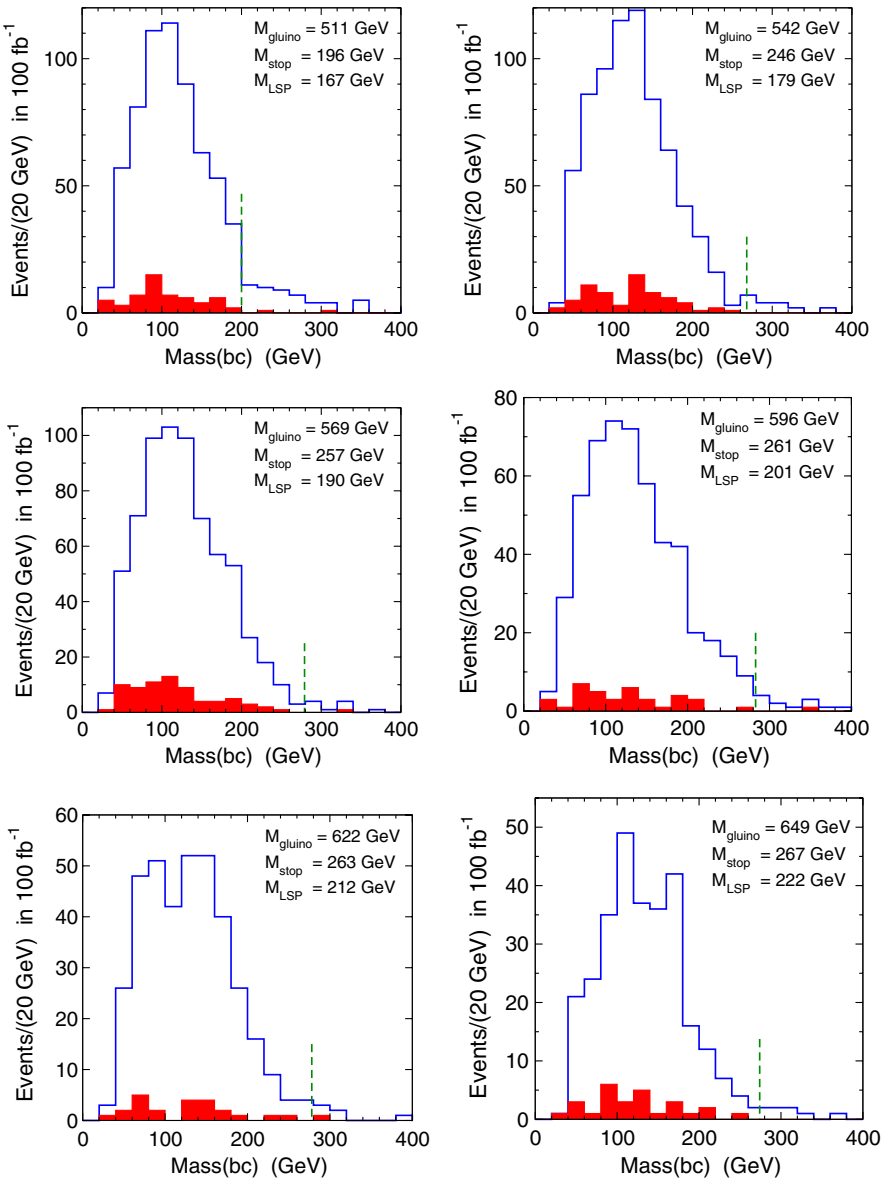

FIG. 11 (color online). The distributions of $m(bc)$ for six points on the model line described in Sec. II with $M_1 = 425, 450, 475, 500, 525$, and 550 GeV. The nominal endpoints, indicated by the dashed vertical lines, are given by Eq. (5.2) as, respectively, $m(bc)_{\max} = 200, 268, 279, 283, 278$, and 274 GeV. The solid histograms show the portion of the signal for which the putative c jet has a heavy-flavor tag or a soft muon tag.

representative models. These distributions are seen to be roughly consistent with endpoints at the nominal positions, but wrong assignments and jet energy smearing leads to some events in a high-mass tail in each case. This can be seen to be particularly troublesome for the lowest-mass $M_1 = 425$ GeV ($m_{\tilde{g}} = 511$) model point, where the small mass difference $m_{\tilde{t}_1} - m_{\tilde{N}_1} = 29$ GeV means that the true charm jets often fail the $p_T > 35$ GeV cut.[4] This exemplifies a more general difficulty. If the thermal relic abundance of neutralinos does not account for all of the dark matter, then the stop-LSP mass difference will be smaller than indicated in Fig. 2, for any given gluino masses. This can always lead to the problem of the charm jets having too small p_T and being replaced in the analysis by interlopers, leading to a distorted distribution and a tail above the true mass endpoint. To counteract this problem, one could use an independent check on the identity of the charm jet. In Figs. 10 and 11, the solid histograms show the portion of the signal for which the putative charm jet has a PGS heavy-flavor tag or contains a nonisolated muon (similar to the ''soft muon'' tag used in Fermilab Tevatron analyses). This information will clearly be more useful if the efficiency

[4]I have checked that lowering this cut does not help significantly, because doing so also allows more interloper jets.

and purity of "charm tagging" can be improved. Although I will not attempt it here in the absence of a fully realistic detector simulation, one can imagine that a likelihood fit taking into account these effects could give measurements (or at least constraints) on these endpoints. However, Figs. 10 and 11 show that precision may be difficult to achieve without either more data than 100 fb^{-1} or a better handle on charm jets.

Unfortunately, even with such a measurement, most of these models are quite indistinguishable from each other using the endpoints or shapes of the distributions alone. This is because the endpoints are nearly independent of the mass scale defining the point along the model line studied here, as illustrated in Fig. 12.

In fact, for the entire range 545 GeV $< m_{\tilde{g}} <$ 830 GeV, $m(b\ell c)_{\text{max}}$ is within 10 GeV of 350 GeV for this model line. (For lower values of the gluino mass, the endpoint is lower, but its determination becomes much more problematic because of wrong jet assignments due to the smaller stop-LSP mass difference, as we have just seen.) It might at first seem surprising that the position of the endpoints does not scale with the gluino mass. The reason is that the scaling is counteracted by the factor of $(1 - m^2_{\tilde{N}_1}/m^2_{\tilde{t}_1})$ in Eqs. (5.1), (5.2), and (5.3), which decreases as one moves to higher masses along the model line, because of the constraint on the stop-LSP mass difference coming from the dark-matter abundance observation.

Nevertheless, a successful determination of the endpoints will still be useful when combined with the information that the gluino decay signal is kinematically allowed at all. This is illustrated in Fig. 13, which assumes that the $m(b\ell c)$ endpoint is found to be 350 GeV [or equivalently that the $m(bc)$ endpoint is found at 279 GeV].

The allowed line in the gluino mass vs stop mass plane is shown, for various assumptions about the stop-LSP mass

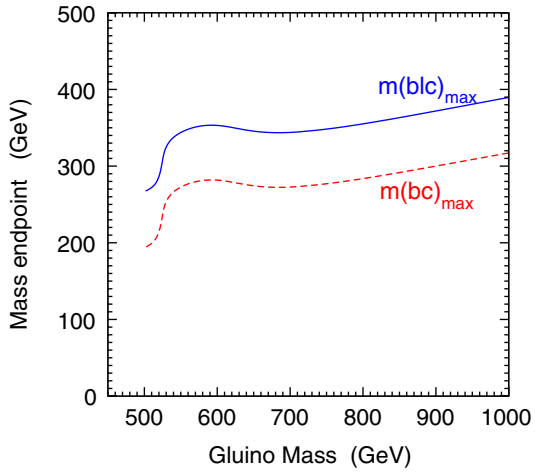

FIG. 12 (color online). The parton-level prediction for the endpoints of the $m(b\ell c)$ and $m(bc)$ distributions, for points along the model line described in Sec. II, as a function of the gluino mass.

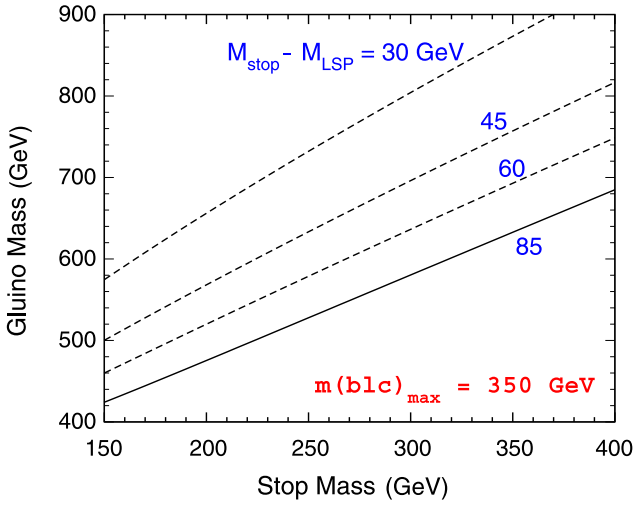

FIG. 13 (color online). The relation between the gluino ($\tilde{g}$) and the lighter stop ($\tilde{t}_1$) masses following from Eq. (5.3), for the case that the high endpoint of the $m(b\ell c)$ distribution is taken to be 350 GeV. The different lines correspond to $m_{\tilde{t}_1} - m_{\tilde{N}_1} = 30$, 45, 60, and 85 GeV. The last is the maximum mass difference that allows $\tilde{t}_1 \to c\tilde{N}_1$ to dominate, as required by the signal.

difference. For the signal to occur at all, one must have $m_{\tilde{t}_1} - m_{\tilde{N}_1} < 85$ GeV; otherwise the decay $\tilde{t}_1 \to c\tilde{N}_1$ would lose to the flavor-preserving 3-body decay $\tilde{t}_1 \to bW\tilde{N}_1$. (As noted at the end of Sec. III, this can be ruled out by counting the number of additional heavy-flavor tags in the events that pass the signal selections.) This means that for a given stop mass, the gluino mass must be above the solid line. The dashed lines show the gluino-stop mass relation for smaller values of the $m_{\tilde{t}_1} - m_{\tilde{N}_1}$ mass difference. [If the $m(b\ell c)$ endpoint is only constrained to be ≥ 350 GeV, then the allowed regions are above the indicated lines.] Now, combining this information with an estimate or upper bound on the gluino mass from the production cross section or from the observables of the type $M_{A,B,C,D}$ described above would allow a determination of ranges in which the gluino, stop, and LSP masses must be.

VI. OUTLOOK

Compressed supersymmetry with top-squark mediation of neutralino annihilation in the early universe presents both challenges and opportunities for the LHC. Although early discovery should not be a problem because of the low mass scale, the sleptons and the charginos and neutralinos (other than the LSP) may very nearly decouple. In the model line studied here, for example, it is very difficult and perhaps impossible for the LHC to be able to say anything about them. With sufficient integrated luminosity, one may be able to discover stoponium through its diphoton decays [39,59], giving a uniquely precise measurement of the top-squark mass. This would provide an important

absolute reference point for determination of the other superpartner masses. However, it requires that the top-squark mass is not too large.

Other than stoponium, the most distinctive signature may be the same-sign leptonic top-quark decays that come from gluinos (or squarks decaying to gluinos). In this paper, I have studied the prospects for learning about the gluino, top-squark, and LSP masses from these events.

First, the scenario is distinguishable from similar ones with a larger stop-LSP mass difference by using the frequency of additional heavy-flavor tags in the $\ell^{\pm}\ell^{\pm}bbjj + E_T^{\rm miss}$ events after cuts.

Observables obtained by summing over scalar p_T's and $E_T^{\rm miss}$ within this relatively clean sample will provide estimates of the effective superpartner mass scale, which is always strongly correlated with the gluino mass. This can be compared with the estimate obtained from H_T and $M_{\rm eff}$ distributions in the larger inclusive jets + $E_T^{\rm miss}$ sample.

The determination of invariant mass endpoints is somewhat more problematic, due to the pernicious effects of interloping jets (both from squark decays and from the underlying event) being confused with the charm jet in the analysis. In the actual LHC analysis, this can probably be enhanced by using heavy-flavor likelihoods on an event-by-event basis to help choose the correct charm jets. These endpoints do not provide unambiguous information about the superpartner masses, even within the confines of the single model line studied here. However, when combined with the information that the decay $\tilde{t}_1 \rightarrow c\tilde{N}_1$ dominates, this information can also be useful to constrain the model. Clearly, heavy-flavor tagging will be crucial in this effort. Also, if one is willing to assume that the thermal relic abundance of dark matter is due entirely to neutralino LSPs without fine-tuning, then the resulting stop-LSP mass difference should be large enough to more sharply define the endpoints. Conversely, a confirmation of this scenario would help to establish the supersymmetric interpretation of the dark matter.

ACKNOWLEDGMENTS

I am indebted to John Conway, Dave Hedin, Michel Herquet, Gudrun Hiller, Tilman Plehn, and Tim Stelzer for helpful communications. This work was supported in part by the National Science Foundation Grant No. PHY-0456635. This research was supported in part by the National Science Foundation under Grant No. PHY05-51164.

[1] For reviews of supersymmetry at the TeV scale, see S. P. Martin, arXiv:hep-ph/9709356; M. Drees, R. Godbole, and P. Roy, *Theory and Phenomenology of Sparticles: An Account of Four-Dimensional $N = 1$ Supersymmetry in High Energy Physics* (World Scientific, Singapore, 2004); H. Baer and X. Tata, *Weak Scale Supersymmetry: From Superfields to Scattering Events* (Cambridge University Press, Cambridge, England, 2006).

[2] ATLAS Collaboration, Report No. CERN-LHCC-99-15, Report No. ATLAS-TDR-15, 1999.

[3] CMS Collaboration, Report No. CERN-LHCC-2006-001, Report No. CMS TDR 8.1, 2006.

[4] S. P. Martin, Phys. Rev. D **75**, 115005 (2007); **76**, 095005 (2007).

[5] D. N. Spergel *et al.* (WMAP Collaboration), Astrophys. J. Suppl. Ser. **170**, 377 (2007); E. Komatsu *et al.* (WMAP Collaboration), arXiv:astro-ph/0803.0547.

[6] M. Tegmark *et al.* (SDSS Collaboration), Phys. Rev. D **69**, 103501 (2004); **74**, 123507 (2006).

[7] J. R. Ellis, K. Enqvist, D. V. Nanopoulos, and K. Tamvakis, Phys. Lett. **155B**, 381 (1985).

[8] M. Drees, Phys. Lett. **158B**, 409 (1985).

[9] G. Anderson, C. H. Chen, J. F. Gunion, J. D. Lykken, T. Moroi, and Y. Yamada, arXiv:hep-ph/9609457.

[10] G. Anderson, H. Baer, C. h. Chen, and X. Tata, Phys. Rev. D **61**, 095005 (2000).

[11] G. L. Kane and S. F. King, Phys. Lett. B **451**, 113 (1999); M. Bastero-Gil, G. L. Kane, and S. F. King, Phys. Lett. B **474**, 103 (2000).

[12] A. Corsetti and P. Nath, Phys. Rev. D **64**, 125010 (2001); **66**, 035003 (2002).

[13] A. Birkedal-Hansen and B. D. Nelson, Phys. Rev. D **64**, 015008 (2001); **67**, 095006 (2003).

[14] H. Baer *et al.*, J. High Energy Phys. 05 (2002) 061;

[15] V. Bertin, E. Nezri, and J. Orloff, J. High Energy Phys. 02 (2003) 046.

[16] U. Chattopadhyay and D. P. Roy, Phys. Rev. D **68**, 033010 (2003).

[17] D. G. Cerdeño and C. Muñoz, J. High Energy Phys. 10 (2004) 015.

[18] G. Belanger, F. Boudjema, A. Cottrant, A. Pukhov, and A. Semenov, Nucl. Phys. **B706**, 411 (2005); Czech. J. Phys. **55**, B205 (2005).

[19] Y. Mambrini and E. Nezri, Eur. Phys. J. C **50**, 949 (2007).

[20] S. F. King and J. P. Roberts, J. High Energy Phys. 09 (2006) 036; 01 (2007) 024.

[21] H. Baer, A. Mustafayev, E. K. Park, S. Profumo, and X. Tata, J. High Energy Phys. 04 (2006) 041; H. Baer, A. Mustafayev, S. Profumo, and X. Tata, Phys. Rev. D **75**, 035004 (2007).

[22] N. Arkani-Hamed, A. Delgado, and G. F. Giudice, Nucl. Phys. **B741**, 108 (2006).

[23] A. Falkowski, O. Lebedev, and Y. Mambrini, J. High Energy Phys. 11 (2005) 034.

[24] M. Perelstein and C. Spethmann, J. High Energy Phys. 04 (2007) 070.

[25] J. R. Ellis, K. A. Olive, and P. Sandick, Phys. Lett. B **642**, 389 (2006); J. High Energy Phys. 06 (2007) 079.

[26] H. Baer, E. K. Park, X. Tata, and T. T. Wang, J. High Energy Phys. 08 (2006) 041; 06 (2007) 033.
[27] K. J. Bae, R. Dermisek, H. D. Kim, and I. W. Kim, J. Cosmol. Astropart. Phys. 08 (2007) 014.
[28] S. F. King, J. P. Roberts, and D. P. Roy, J. High Energy Phys. 10 (2007) 106.
[29] D. Feldman, Z. Liu, and P. Nath, Phys. Rev. Lett. **99**, 251802 (2007); **100**, 069902(E) (2008); Phys. Lett. B **662**, 190 (2008); J. High Energy Phys. 04 (2008) 054.
[30] H. Baer, A. Mustafayev, H. Summy, and X. Tata, J. High Energy Phys. 10 (2007) 088.
[31] H. Baer, A. Mustafayev, E. K. Park, and X. Tata, J. High Energy Phys. 05 (2008) 058.
[32] R. H. K. Kadala, P. G. Mercadante, J. K. Mizukoshi, and X. Tata, arXiv:hep-ph/0803.0001.
[33] L. L. Everett, I. W. Kim, P. Ouyang, and K. M. Zurek, arXiv:hep-ph/0804.0592 [Phys. Rev. Lett. (to be published)]; arXiv:hep-ph/0806.2330.
[34] K.-i. Hikasa and M. Kobayashi, Phys. Rev. D **36**, 724 (1987).
[35] C. Boehm, A. Djouadi, and Y. Mambrini, Phys. Rev. D **61**, 095006 (2000).
[36] V. D. Barger, W. Y. Keung, and R. J. N. Phillips, Phys. Rev. Lett. **55**, 166 (1985); R. M. Barnett, J. F. Gunion, and H. E. Haber, Phys. Lett. B **315**, 349 (1993); H. Baer, X. Tata, and J. Woodside, Phys. Rev. D **41**, 906 (1990).
[37] S. Kraml and A. R. Raklev, Phys. Rev. D **73**, 075002 (2006).
[38] H. Baer, A. Box, E. K. Park, and X. Tata, J. High Energy Phys. 08 (2007) 060.
[39] S. P. Martin, Phys. Rev. D **77**, 075002 (2008).
[40] B. C. Allanach, Comput. Phys. Commun. **143**, 305 (2002).
[41] G. Belanger, F. Boudjema, A. Pukhov, and A. Semenov, Comput. Phys. Commun. **176**, 367 (2007); **174**, 577 (2006); **149**, 103 (2002).
[42] M. Muhlleitner, A. Djouadi, and Y. Mambrini, Comput. Phys. Commun. **168**, 46 (2005).
[43] S. P. Das, A. Datta, and M. Guchait, Phys. Rev. D **65**, 095006 (2002).
[44] G. Hiller and Y. Nir, J. High Energy Phys. 03 (2008) 046.
[45] I. Hinchliffe, F. E. Paige, M. D. Shapiro, J. Soderqvist, and W. Yao, Phys. Rev. D **55**, 5520 (1997); H. Bachacou, I. Hinchliffe, and F. E. Paige, Phys. Rev. D **62**, 015009 (2000).
[46] B. C. Allanach, C. G. Lester, M. A. Parker, and B. R. Webber, J. High Energy Phys. 09 (2000) 004.
[47] J. Hisano, K. Kawagoe, R. Kitano, and M. M. Nojiri, Phys. Rev. D **66**, 115004 (2002); J. Hisano, K. Kawagoe, and M. M. Nojiri, Phys. Rev. D **68**, 035007 (2003).
[48] B. K. Gjelsten, D. J. Miller, and P. Osland, J. High Energy Phys. 12 (2004) 003; D. J. Miller, P. Osland, and A. R. Raklev, J. High Energy Phys. 03 (2006) 034.
[49] C. G. Lester, M. A. Parker, and M. J. White, J. High Energy Phys. 01 (2006) 080.
[50] C. Boehm, A. Djouadi, and M. Drees, Phys. Rev. D **62**, 035012 (2000); J. R. Ellis, K. A. Olive, and Y. Santoso, Astropart. Phys. **18**, 395 (2003); C. Balazs, M. Carena, and C. E. M. Wagner, Phys. Rev. D **70**, 015007 (2004); C. Balazs, M. S. Carena, A. Menon, D. E. Morrissey, and C. E. M. Wagner, Phys. Rev. D **71**, 075002 (2005); G. Belanger, F. Boudjema, S. Kraml, A. Pukhov, and A. Semenov, Phys. Rev. D **73**, 115007 (2006).
[51] PROSPINO 2.0, available at http://www.ph.ed.ac.uk/~tplehn/prospino/, uses results found in W. Beenakker, R. Hopker, M. Spira, and P. M. Zerwas, Nucl. Phys. **B492**, 51 (1997); W. Beenakker, M. Kramer, T. Plehn, M. Spira, and P. M. Zerwas, Nucl. Phys. **B515**, 3 (1998); W. Beenakker, M. Klasen, M. Kramer, T. Plehn, M. Spira, and P. M. Zerwas, Phys. Rev. Lett. **83**, 3780 (1999); **100**, 029901(E) (2008); M. Spira, arXiv:hep-ph/0211145; T. Plehn, Czech. J. Phys. **55**, B213 (2005).
[52] J. Hubisz, J. Lykken, M. Pierini, and M. Spiropulu, arXiv:hep-ph/0805.2398 [Phys. Rev. D (to be published)].
[53] H. Baer, C. Balazs, A. Belyaev, T. Krupovnickas, and X. Tata, J. High Energy Phys. 06 (2003) 054.
[54] C. G. Lester and D. J. Summers, Phys. Lett. B **463**, 99 (1999); A. Barr, C. Lester, and P. Stephens, J. Phys. G **29**, 2343 (2003).
[55] W. S. Cho, K. Choi, Y. G. Kim, and C. B. Park, Phys. Rev. Lett. **100**, 171801 (2008); B. Gripaios, J. High Energy Phys. 02 (2008) 053; A. J. Barr, B. Gripaios, and C. G. Lester, J. High Energy Phys. 02 (2008) 014; W. S. Cho, K. Choi, Y. G. Kim, and C. B. Park, J. High Energy Phys. 02 (2008) 035.
[56] J. Alwall *et al.*, J. High Energy Phys. 09 (2007) 028; F. Maltoni and T. Stelzer, J. High Energy Phys. 02 (2003) 027; T. Stelzer and W. F. Long, Comput. Phys. Commun. **81**, 357 (1994).
[57] T. Sjostrand, S. Mrenna, and P. Skands, J. High Energy Phys. 05 (2006) 026.
[58] John Conway *et al.*, http://www.physics.ucdavis.edu/~conway/research/software/pgs/pgs4-general.htm. See also http://v1.jthaler.net/olympicswiki/doku.php?id=lhc_olympics:particle_identification.
[59] M. Drees and M. M. Nojiri, Phys. Rev. Lett. **72**, 2324 (1994); Phys. Rev. D **49**, 4595 (1994).